Title

Ectopic Production of 3,4-Dihydroxybenzoate in Planta Affects Cellulose Structure and Organization

Permalink

https://escholarship.org/uc/item/9mp34528

Journal

Biomacromolecules, 25(6)

ISSN

1525-7797

Authors

Senanayake, Manjula

Lin, Chien-Yuan

Mansfield, Shawn D

et al.

Publication Date

2024-06-10

DOI

10.1021/acs.biomac.4c00187

Copyright Information

Peer reviewed

Ectopic Production of 3,4-Dihydroxybenzoate *in Planta* Affects Cellulose Structure and Organization

Manjula Senanayake, Chien-Yuan Lin, Shawn D. Mansfield, Aymerick Eudes, Brian H. Davison, Sai Venkatesh Pingali,* and Hugh O'Neill*

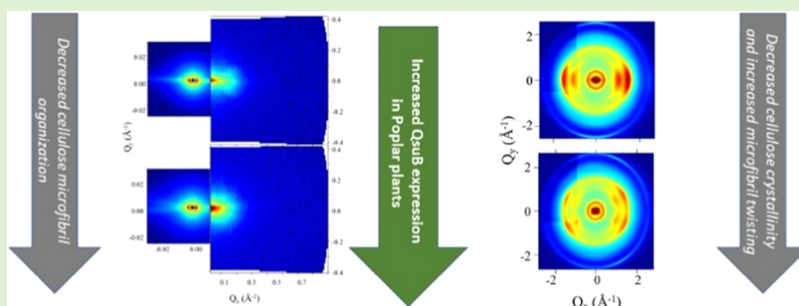Cite This: *Biomacromolecules* 2024, 25, 3542−3553

Read Online

ACCESS | Metrics & More | Article Recommendations | Supporting Information

ABSTRACT: Lignocellulosic biomass is a highly sustainable and largely carbon dioxide neutral feedstock for the production of biofuels and advanced biomaterials. Although thermochemical pretreatment is typically used to increase the efficiency of cell wall deconstruction, genetic engineering of the major plant cell wall polymers, especially lignin, has shown promise as an alternative approach to reduce biomass recalcitrance. Poplar trees with reduced lignin content and altered composition were previously developed by overexpressing bacterial 3-dehydroshikimate dehydratase (QsuB) enzyme to divert carbon flux from the shikimate pathway. In this work, three transgenic poplar lines with increasing QsuB expression levels and different lignin contents were studied using small-angle neutron scattering (SANS) and wide-angle X-ray scattering (WAXS). SANS showed that although the cellulose microfibril cross-sectional dimension remained unchanged, the ordered organization of the microfibrils progressively decreased with increased QsuB expression. This was correlated with decreasing total lignin content in the QsuB lines. WAXS showed that the crystallite dimensions of cellulose microfibrils transverse to the growth direction were not affected by the QsuB expression, but the crystallite dimensions parallel to the growth direction were decreased by ∼20%. Cellulose crystallinity was also decreased with increased QsuB expression, which could be related to high levels of 3,4-dihydroxybenzoate, the product of QsuB expression, disrupting microfibril crystallization. In addition, the cellulose microfibril orientation angle showed a bimodal distribution at higher QsuB expression levels. Overall, this study provides new structural insights into the impact of ectopic synthesis of small-molecule metabolites on cellulose organization and structure that can be used for future efforts aimed at reducing biomass recalcitrance.

■ INTRODUCTION

Plants convert atmospheric carbon dioxide into carbohydrates through photosynthetic carbon dioxide fixation that can then be deposited and stored in the plant cell wall.[1] During the early stages of plant cell development, the primary wall is first deposited and is composed principally of cellulose, hemicellulose, and pectin.[2] As the plant matures, this is followed by the deposition of a secondary wall that largely consists of cellulose, hemicellulose, and the polyphenolic polymer lignin.[3] Due to the high abundance of cellulose and lignin in plant cell walls, the biomass from mature plants enriched in secondary cell walls is termed lignocellulose. The significant amount of solar energy that is stored in lignocellulose is an important resource that can be used for clean energy and biomaterial production. However, only about 4% of globally produced lignocellulosic biomass is employed for applications that

include cooking, heating, construction materials, and the paper industry.[4] In recent decades, lignocellulosic biomass has been extensively studied as a sustainable source of bioenergy and renewable bioproducts.[5,6] This has led to the development of enabling conversion technologies that facilitate the extraction of energy-rich sugars and polymers from plant cell walls.[5] However, making the conversion process cost-effective remains a challenge as plant cell walls are inherently resistant to microbial and enzymatic deconstruction.[7] This is
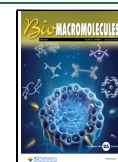
known as "biomass recalcitrance" and is the collective result of the encapsulation of energy-rich cellulose and hemicellulose in the hydrophobic lignin matrix.[8−10]

Lignin is a complex, aromatic biopolymer that constitutes between 10 and 25% of lignocellulosic biomass.[11,12] It surrounds the cellulose microfibril−hemicellulose network and acts as a "cellular glue" providing rigidity to the cell wall.[13] Lignin is composed of three primary monomers: p-hydroxyphenyl (H), guaiacyl (G), and syringyl (S), which are derived from monolignols (p-coumaryl, coniferyl, and sinapyl alcohols).[14] The S and G units form the backbone of the lignin polymer chains, and their ratio (S/G) can naturally range between 1 and 3.[15−17] A higher S/G ratio is thought to produce longer linear chains of lignin.[18−20] It is known that the amount of lignin in the cell wall, its structure, and its S/G ratio are key factors that impact biomass conversion efficiency.[17,21] The traditional approach to increasing biomass conversion efficiency is the removal of lignin from the biomass prior to the enzymatic hydrolysis reaction, by pretreatment.[22] However, many physical and chemical pretreatment methods lack sustainability as well as practicability for industrial scale-up.[23−25] This has motivated tremendous interest in developing a better understanding of lignin biosynthesis to reduce biomass recalcitrance by modifying lignin content and/or composition through breeding or genetic manipulation.[26]

The monolignols are derived from phenylalanine in the cytosol in a multistep reaction called the phenylpropanoid pathway;[27] phenylalanine biosynthesis occurs inside the plastid.[28] Currently, 10 enzymes are known to be involved in regulating the phenylpropanoid pathway,[29] and another 10 are required for the shikimate pathway.[28] Many studies have demonstrated changes in cell wall structure brought about by altering lignin biosynthesis in mutants and transgenic plants.[27,30] In a previously reported study, the expression of a bacterial 3-dehydroshikimate dehydratase (QsuB) in *Arabidopsis* led to the conversion of 3-dehydroshikimic acid, an intermediate of the shikimate pathway, into 3,4-dihydroxybenzoic acid (DHBA), which is also known as protocatechuic acid.[30] Converting 3-dehydroshikimate into DHBA limits the availability of shikimate, a precursor for lignin biosynthesis and a cofactor of hydroxycinnamoyl transferase, as well as producing an inhibitor of the same transferase.[31,32] This alteration resulted in the reduction of lignin content in the plant cell wall and improved biomass conversion.[30] Recently, this work was extended to study the effects of heterologous expression of QsuB in hybrid poplar (*Populus alba × grandidentata*)[33] to divert carbon flux away from the shikimate pathway.[33] The transgenic poplar wood had up to 33% less lignin with p-hydroxyphenyl units comprising as much as 10% of the lignin. Cell wall compositional analysis shows that transgenic poplar wood released fewer ester-linked p-hydroxybenzoate groups than wild-type trees and revealed the novel incorporation of cell-wall-bound dihydroxybenzoate esters as well as glycosides of DHBA. Furthermore, the participation of monolignol−dihydroxybenzoate conjugates in lignification was also proposed to explain the occurrence of pendent DHBA moieties on the lignin, as well as backbone-integrated DHBA units, ultimately producing a novel type of "zip-lignin." In addition, up to 40% more glucose was released from the QsuB expressing poplar lines following ionic liquid pretreatment and enzymatic hydrolysis.[33]

Understanding the structure and organization of the plant cell wall is critical in designing an optimal, sustainable, and reliable approach for improving biomass conversion. For instance, dilute acid pretreatment was originally developed to hydrolyze hemicelluloses and then expose cellulose for improved glucose release.[34] However, several structural studies showed that acidic aqueous solvents also increased the propensity of cellulose to coalesce[35] and lignin to aggregate, thereby limiting the effectiveness of the approach.[36] Similarly genetic approaches to alter the lignin content may have unintended consequences for the structure of the plant cell walls. Determining how the cell wall structure changes can inform about the effects of downstream processing for deconstructing the biomass and provide valuable insights into the limitations of a particular approach.

This study investigates the structural changes in the cell walls of transgenic QsuB hybrid poplar using small-angle neutron scattering (SANS) and wide-angle X-ray scattering (WAXS) to understand previously reported increased saccharification in these transgenic plants.[33,37] SANS measures the structural changes in cellulose microfibril dimensions, microfibril packing, and the structure of the copolymer matrix on length scales between ∼1 and 600 nm. In contrast, WAXS measures the structure of the cellulose microfibrils themselves and can provide information about the orientation of the cellulose chains, cellulose crystallinity, and cellulose crystal dimensions. Our results show significant structural changes in the meso-scale structure of the cellulose microfibrils with increasing QsuB expression, supporting an important role for lignin in maintaining the structural integrity of the cell wall. The atomic scale structure of the crystalline cellulose microfibrils is also affected by QsuB expression, exhibiting a decrease in crystallinity that is evident along the length of the microfibrils. Overall, this study provides structural insight how altered lignin biosynthesis and accumulation of DHBA or derivatives affects the plant cell wall structure. These data may help future development of transgenic plants aimed at reducing biomass recalcitrance for the production of fuels and chemicals.

■ MATERIALS AND METHODS

Biomass Samples. Wood from three different poplar transgenic lines (QsuB1, QsuB5, and QsuB15) with reduced lignin content and wild type (WT) were grown in controlled conditions at the Joint BioEnergy Institute (JBEI), Emeryville, CA, as previously described.[37] The harvested stems were debarked and air-dried (see Figure S1). The stems were cut into eight pieces approximately 10 cm in length (see Figure S1C); the bottom 0.5 cm (#1) was used for SANS and WAXS evaluation.

SANS and WAXS Sample Preparation. Thin sliced wood pieces were obtained by slicing along the growth direction of the stem using a razor blade. This preserved the natural alignment of the cellulose microfibrils in the native plant cell walls. The bottom (#1) stem piece of the poplar wood was sliced into multiple 1 mm-thick slices and immersed in 100% D_2O solvent to exchange hydrogen and deuterium atoms to achieve maximum contrast between cell wall components and solvent. The first two soaks were for 1−2 h. The third soak duration was overnight, and the fourth and final soak was 2 h before the samples were loaded into the SANS titanium cells with detachable windows. About 3−5 slices per sample were carefully placed side-by-side with each slice vertically aligned in the sample cell.

Samples for WAXS measurements were also 1 mm-thick slices and sliced along the stem growth direction of the bottom (#1) stem piece. To remove water with minimal disruption to the cell wall structure, these samples were freeze-dried for five days prior to placing the slices vertically into 1.5 mm diameter quartz capillaries to perform WAXS measurements.
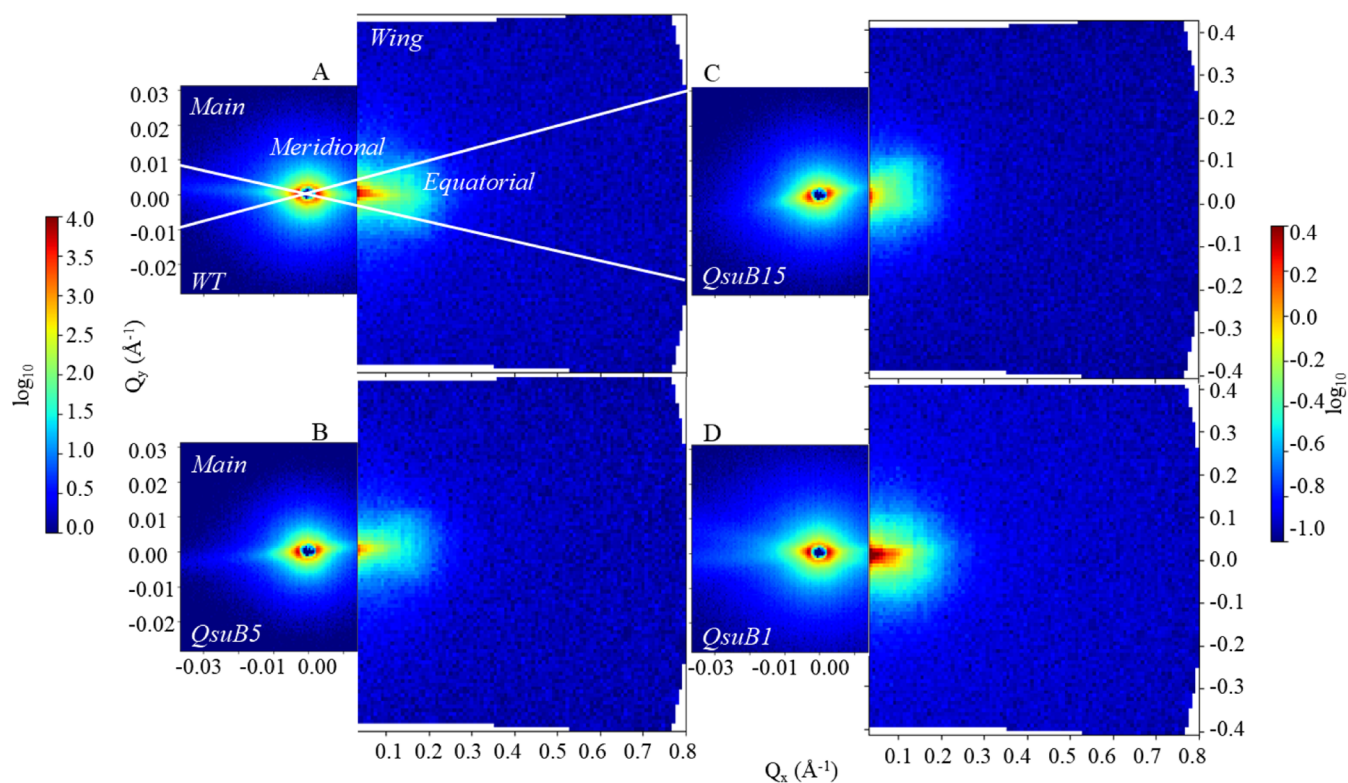
Figure 1. 2D SANS detector images of intact native WT (A) and transgenic QsuB5 (B), and QsuB15 (C) and QsuB1 (D) poplar stem samples in 100% D_2O solvent. Each panel shows the main (left) and wing (right) detector images from the Bio-SANS instrument. Lines in panel A represent the equatorial and meridional sectors that were used for data analysis and interpretation. The intensity scale bars shown on the left and right refer to the main and wing detector, respectively.

SANS Data Collection and Analysis. SANS measurements of WT and QsuB transgenic trees were performed at the Bio-SANS instrument located at the High Flux Isotope Reactor (HFIR) in the Oak Ridge National Laboratory (ORNL). The main detector array was at 15.5 m from the sample position, and the curved wing detector array at 1.13 m from the sample was rotated to 1.4° from the direct beam. Using this detector configuration, the Q ranges obtained using 6 and 18 Å neutrons were $0.003 < Q\,(\text{Å}^{-1}) < 0.8$ and $0.001 < Q\,(\text{Å}^{-1}) < 0.1$, respectively, and combined to obtain an overall Q range of 0.001 to 0.8 Å^{-1}. The wavelength spread $(\Delta\lambda/\lambda)$ was 13.2%.

The D_2O exchanged stem slices described above were placed in a vertical orientation in the titanium sample holders perpendicular to the neutron beam to capture the scattering signal from the cellulose microfibrils on the wing detector. The samples produced an anisotropic two-dimensional (2D) scattering pattern (Figure 1). The raw 2D images were processed by normalizing to the incident beam monitor counts, correcting for detector dark current and pixel sensitivity, and subtracting scattering contribution from the quartz cell and D_2O buffer. Two scattering intensity profiles $I(Q)$ versus Q were obtained from the equatorial (wedge 0) and meridional (wedge 1) sectors of the 2D image (Figure S2). The scattering from the matrix copolymer is isotropic and observed in both the equatorial and meridional sectors. The scattering of the cellulose microfibrils aligned parallel along the stem growth direction dominates in the equatorial sector. To isolate the scattering features of cellulose microfibrils aligned along the growth direction (perpendicular to the beam), the meridional scattering contribution was subtracted from the equatorial sector.

The SANS data were analyzed using the Modeling II tool implemented in the Irena package[38] in Igor Pro 8.0 software (by WaveMetrics) to elucidate plant cell wall structure. The basic small-angle scattering formula for scattered intensity $I(Q)$ is,

$$I(Q) = |\Delta\rho|^2 S(Q) \int_0^\infty |F(Q, R)|^2 V(R)^2 NP(R)\mathrm{d}R \tag{1}$$

where $|\Delta\rho|$ is the contrast between the scattering particle and solvent $|\rho_{\text{particle}} - \rho_{\text{solvent}}|$, $F(Q, R)$ is the scattering form factor of the cylindrical particles, $V(R)$ is the particle volume of size R, N is the total number of scattering particles, $P(R)$ is the Gaussian probability density distribution of the scattering particles of size R, and $S(Q)$ is the structure factor modeled as hard sphere structure factor. The hard sphere structure factor is robust for spherical particles, but for particle shapes that deviate from a spherical shape like in the current study, the hard sphere structure factor performs reasonably for low degree of correlation. The equatorial SANS profiles were fit using a cylindrical form factor in the high-Q region $(Q > 0.025\ \text{Å}^{-1})$ for all samples to represent cellulose microfibril dimensions. The mathematical formulation of the cylindrical form factor and structure factor for a weakly correlated system of cylinders is given by

$$P(Q) = \frac{\phi}{V_{\text{cyl}}} \int_o^{\pi/2} f^2(Q, \alpha)\sin\alpha\ \mathrm{d}\alpha \tag{2}$$

$$f(Q, \alpha) = 2(\rho_{\text{cyl}} - \rho_{\text{solv}})V_{\text{cyl}}j_0(QH\cos\alpha)\frac{J_1(QR_{\text{cs}}\sin\alpha)}{(QR_{\text{cs}}\sin\alpha)} \tag{3}$$

$$S(Q) = \frac{1}{1 + k\frac{3(\sin(Q\zeta) - Q\zeta\cos(Q\zeta))}{(Q\zeta)^3}} \tag{4}$$

$$j_0(x) = \frac{\sin x}{x} \tag{5}$$

$$V_{\text{cyl}} = \pi R_{\text{cs}}^2(2H) \tag{6}$$

where ϕ is the volume fraction of the cylinder particles, V_{cyl} is the volume of a cylinder with cross-sectional radius R_{cs} and length L $(=2H)$, α is the orientation angle of the cylinder's long axis, and J_1 is a first-order Bessel function. The fit parameters of the structure factor, $S(Q)$, are k, the degree of packing (also referred to as the packing
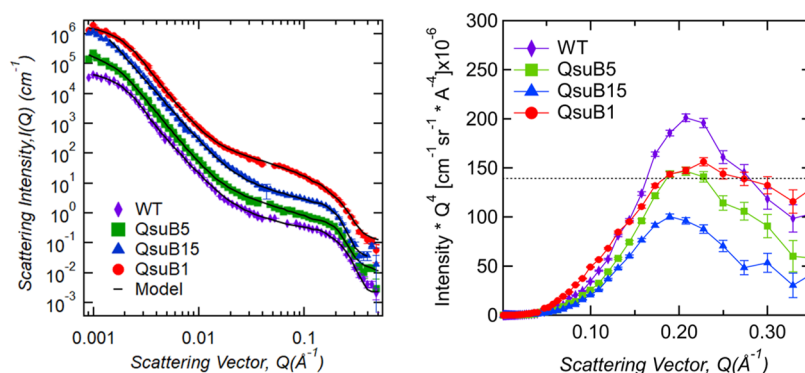
Figure 2. (A) 1D SANS equatorial profiles of WT (purple diamond), QsuB5 (green square), QsuB15 (blue triangle), and QsuB1 (red circle). Except for WT, all the profiles were scaled by a factor of 10 for clarity. Unscaled data are given in Figure S3-A. (B) Porod plot showing the high-Q region of WT and transgenic lines (not scaled).

factor), and ζ, the center-to-center distance between particles. The structure factor, as given in eq 4, in this study, accounts for weak cylinder–cylinder correlation and is used to model the correlation between cellulose microfibrils. The packing factor k represents the density of packing of cellulose microfibrils and provides a measure of their correlations, and ζ is interpreted as center-to-center distance between cellulose microfibrils. When the fit value of the packing factor $k < 4$,[39] the fit indicates weak correlations. The low-Q data ($Q < 0.025$ Å^{-1}) was fit to a Unified function, given by

$$I(Q) = G \times \exp\left(-\frac{Q^2 R_g^2}{3}\right) + B \times Q^{-P},$$ where P is the power-law exponent of the scattering curves, R_g is the radius of gyration of the scattering particle, and G and B are the scale factors of the Guinier and power-law functions, respectively. For the subtracted equatorial one-dimensional (1D) SANS profiles of WT, QsuB5, and QsuB15, a structure factor was included to obtain the best fit. For the equatorial 1D SANS profile of QsuB1, no structure factor was required to obtain the best fit, and the convergence of the fit using least-square fit (LSQF)[40] was based of minimizing the chi-squared (χ^2) value of the fit for the entire data range.

The meridional SANS data were modeled by using a three-level fit. The high-Q ($Q > 0.075$ Å^{-1}) region was modeled by the spherical form factor given as

$$P(q) = \frac{\phi}{V_{sph}} \frac{3[\sin(Q) - QR_{sph}\cos(QR_{sph})]^2}{(QR_{sph})^3} \tag{7}$$

where ϕ is the volume fraction of spheres and $V_{sph} = \frac{4}{3}\pi R_{sph}^3$ is the volume of a sphere of radius R_{sph}. In addition, two slopes were observed in the intermediate Q region ($0.01 < Q < 0.075$ Å^{-1}) and low-Q region ($0.001 < Q < 0.01$ Å^{-1}), and those two levels were fit using the Unified fit described above.

WAXS Data Collection and Analysis. The freeze-dried poplar stems were used to acquire WAXS data on a Xenocs Xeuss 3.0 instrument equipped with a D2+ MetalJet X-ray source (Ga K, 9.2 keV, $\lambda = 1.341$ Å). The stems were placed vertically in the X-ray beam and measured in transmission mode. The scattered beam was recorded on a Dectris Eiger 2R 4 M hybrid photon counting detector with a pixel dimension of 75×75 μm^2. The 2D WAXS images, collected as 3-min exposures, were reduced using sectors similar to the approach described for the SANS data above to produce 1D WAXS profiles, scattering intensity vs. scattering vector, Q. The WAXS data were placed on an absolute intensity scale (cm^{-1}) using the direct beam as the intensity calibration. The 2D WAXS patterns of different samples are shown in Figure 5.

WAXS data provides information about cellulose chain organization in cellulose microfibrils. The crystalline characteristics such as crystallite size and crystallinity were estimated using the peak fitting method using Fityk software.[41] Crystallinity was calculated as the ratio of crystalline area to the total area in each analyzed sector of the

WAXS profile. The crystallite size was determined by applying the Scherrer equation for symmetrically shaped crystallites to the WAXS peaks and given by eqs 9 and 10, respectively.[42]

$$\%\text{crystallinity} = \frac{(\text{total scattering area} - \text{amorphous area})}{\text{total scattering area}} \times 100 \tag{9}$$

$$t = (0.9 \times \lambda) \div (\beta \cos\theta) \tag{10}$$

Here, t is the crystallite size, the constant 0.9 represents a dimensionless shape factor for symmetrically shaped crystallites, λ is the wavelength of the incident beam, and β and θ are the values for full-width at half-maximum (FWHM in radians) and peak position in 2θ, respectively.

Production and Purification of Bacterial Cellulose. Bacterial cellulose was grown for 5 days using a previously reported method[43] in the presence of 0, 0.31, 0.77, 1.16, and 1.54 mg/100 mL DHBA in the culture medium. The pellicle that formed at air–liquid interface was removed and washed rigorously and repeatedly with water at 4 °C to remove the growth media and the bacterial debris. The pellicles were then frozen at −80 °C for 2h followed by grinding using a Warburg blender to form a slurry. The homogeneous slurry was then freeze-dried for 3 days to remove the water before performing the WAXS measurements.

■ RESULTS

Composition of Cell Wall Components in QsuB Mutants. The transgenic poplar lines were generated by the introduction of 3-dehydroshikimate dehydratase (QsuB), as described previously.[33,37] The level of QsuB expression in the different transgenic lines followed the order: QsuB1 > QsuB15 > QsuB5 > WT (which was zero, as the gene is not native to plants). The DHBA content in the trees followed the same order while lignin content followed the reverse order as described below. There were visible differences in the appearance and structure of the stems that included a change in color in the hydrated and dried states with increasing QsuB expression level (Figures S1A), and the fibers of the QsuB lines were more easily separated compared to WT trees. This suggests that QsuB expression significantly changes the macroscopic properties and impacts the structural integrity of the trees.

The glucose content (from cellulose), xylose (from xylan hemicellulose), and lignin in WT and the QsuB transgenic plants have been described previously.[33] In summary, the glucose content is similar in all samples, suggesting that QsuB expression does not significantly affect cellulose content. However, both hemicellulose and lignin content were affected

by QsuB expression levels. Xylose content increased approximately from 17 to 21%, and total lignin content decreased from 21 to 14% comparing WT and QsuB1. Furthermore, the S/G ratio of the lignin changed with increasing QsuB expression from 1.8 in the WT to 1.4 in QsuB1. The higher S/G ratio and high H units of lignin monomers usually imply a longer chain length of the lignin polymer[18,19] and higher molecular weight. To understand how the QsuB expression affects cell wall structure at the molecular level, SANS and WAXS studies were performed to obtain structural details of the plant cell walls in the spatial range of 1−600 nm.

SANS Analysis. The 2D SANS scattering patterns of WT stems and the three transgenic lines are shown in Figure 1. The differences in the images can be related to changes in the aligned features in the cell wall due to increased expression of QsuB. For instance, WT and QsuB5 show a sharp streak-like pattern in the equatorial direction with a lobe-like feature that extends to the wing detector image, indicating that the cellulose microfibrils are well-aligned parallel to the stem growth direction. In contrast, the lobe-like features are diminished in the QsuB1 and QsuB15 scattering patterns, which implies that the alignment of the cellulose microfibrils has decreased.

For each 2D scattering pattern, the data were reduced to obtain 1D profiles that represent the equatorial scattering intensity and the meridional sectors shown in Figure 1A. More details of wedge reduction are given in Figure S2 in Supporting Information (SI). The final 1D SANS profiles are shown in Figures 2A and 3. The equatorial SANS profile for the WT
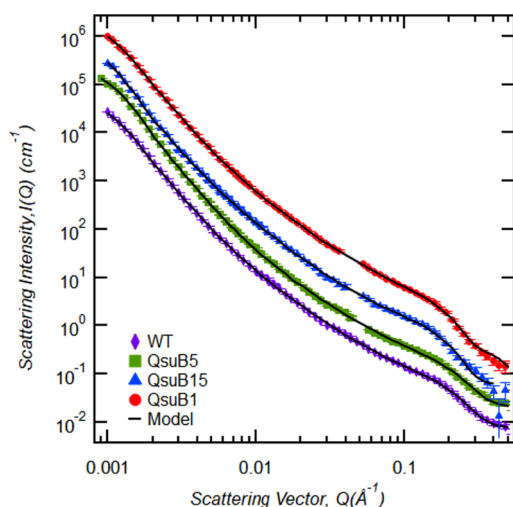

Figure 3. 1D SANS profile of WT (purple diamond), QsuB5 (green square), QsuB15 (blue triangle), and QsuB1 (red circle) meridional scattering. The solid black line represents the model fit. QsuB5, QsuB15, and QsuB1 data are shifted in the y-direction for clarity by a factor of 10. Unscaled data are given in Figure S3-B.

sample shows a sharp well-defined feature ($Q > 0.05$ Å^{-1}) that is attributed to aligned cellulose microfibrils (Figure 2).[44] This feature becomes progressively broader with increasing QsuB expression, as can be observed in the Porod plot (Figure 2B). The peak ($Q = 0.21$ Å^{-1}) in the WT profile, representing the spacing of the aligned cellulose microfibrils, has largely disappeared in the QsuB1 sample (highest QsuB expression),

indicating an absence of alignment of the cellulose microfibrils in this poplar line.

Quantitative analysis was performed using a model that consists of a cylindrical form factor coupled with a structure factor to model the high-Q region (>0.025 Å^{-1}) and a shape-independent unified fit[38] for low-Q region (<0.025 Å^{-1}). The fit parameters are presented in Table 1. The cross-sectional radius of the cylindrical particles representing cellulose microfibrils are similar for the WT and transgenic lines and fall in the range 10−11 Å. This value agrees with the reported cross-sectional size for cellulose microfibrils[45,46] and shows that changes in the QsuB expression level do not alter the cellulose microfibril cross-sectional dimension.

However, the intermicrofibril distance ($d_{spacing}$) between neighboring cellulose microfibrils increased and the packing decreased with increasing QsuB expression levels. The interfibril distance in the WT sample is 30 ± 3 Å with a packing factor of 1.2 ± 0.2, which is similar to previously reported values.[35,47] The value of the packing factor represents the degree of correlation between neighboring cellulose microfibrils. In this case, the value is less than 4, which is consistent with weak correlations between the microfibrils.[39] The microfibril spacing increases to 36 ± 4 Å in QsuB5 with no change in the packing factor. With further increase in QsuB expression, as in the QsuB15 sample, the microfibril spacing increased to 45 ± 6 Å, and the packing factor decreased to 0.9 ± 0. Finally, in the QsuB1 sample, no alignment of the cellulose microfibrils was observed, which agrees with a random organization of cellulose microfibrils.

The observed fits to the low-Q data range indicated that there are large structures with particle sizes greater than 1000 Å, which have smooth surfaces ($P \sim 4$) with a smoothness resolution of 250 Å and do not change with increasing QsuB expression. Several characteristic structures can produce such smooth surface features in the scattering profile, the most probable of which is either the cellulose microfibril bundles or the cell wall lumen.[47]

SANS data in the meridional sector of the 2D pattern originates from the nonaligned components in the plant cell wall such as lignin and hemicellulose (Figure 3). The composite fit model with three levels was used to analyze the data. It is composed of particle size ($Q > 0.075$ Å^{-1}) modeled as spherical particles, a power-law function to represent the amorphous matrix copolymer organization ($0.01 < Q < 0.075$ Å^{-1}), and a second power-law function for features at longest spatial scale, $R_g > 100$ nm ($0.001 < Q < 0.01$ Å^{-1}). The fit parameters are shown in Table 2. Similar to the equatorial SANS curves, the meridional curves also show a shoulder feature in the Level 1 region. SAXS analysis (see the SI for details) of WT stems that were delignified showed that this feature changes significantly with a correlation peak becoming evident as the delignification reaction progresses (SI Figures S4−S7). This is consistent with the scattering contribution from cellulose microfibrils that are oriented perpendicular to the growth direction of the plant (see schematic representation in Figure S8). The SANS data were fit with a spherical form factor to represent the approximately circular cross section of cellulose microfibrils oriented parallel to the incident neutrons. The sphere radius increases with increasing QsuB expression, which may occur because of an increase in misalignment of the neighboring cellulose micro-fibrils and lower lignin content (See SI Figure S8). This is consistent with the increasing interfibril distance and

Table 1. Fitting Parameters Extracted from the 1D Curve Fitting of Equatorial SANS Scattering Profiles

	cylinder				Unified fit	
sample	volume fraction	R_{cs} (Å)	$d_{spacing}$ (Å)	f_{pack}	R_g (Å)	P
Q range (Å^{-1})			0.025−0.4		0.001−0.025	
WT	0.041 ± 0.001	10.0 ± 0.2	30 ± 3	1.2 ± 0.2	1100 ± 78	4.0 ± 0.1
QsuB5	0.039 ± 0.001	10.3 ± 0.2	36 ± 4	1.2 ± 0.1	1200 ± 92	3.9 ± 0.1
QsuB15	0.039 ± 0.001	10.8 ± 0.1	45 ± 6	0.9 ± 0.1	1150 ± 124	4.1 ± 0.1
QsuB1	0.038 ± 0.002	10.4 ± 0.1			1000 ± 103	4.0 ± 0.1

Table 2. Fitting Parameters Extracted from the 1D Curve Fitting of Meridional SANS Scattering Profiles

			power-law exponent	
sample	volume fraction	sphere R_{sph} (Å)	P2	P3
Q range (Å^{-1})		0.075−0.5	0.01−0.075	0.001−0.01
WT	0.004 ± 0.001	11.7 ± 0.1	2.1 ± 0.1	4.2 ± 0.2
QsuB5	0.003 ± 0.001	11.8 ± 0.1	2.1 ± 0.1	4.1 ± 0.1
QsuB15	0.003 ± 0.001	13.7 ± 0.1	2.0 ± 0.1	4.0 ± 0.1
QsuB1	0.004 ± 0.001	14.1 ± 0.1	2.2 ± 0.1	4.1 ± 0.1

decreasing degree of correlation between microfibrils observed for cellulose microfibrils aligned along the plant growth direction. The volume fraction extracted from the analysis also showed that there were ∼10-fold fewer microfibrils aligned in this direction compared to those aligned parallel to the growth direction. The power-law exponent (P) in the second level is interpreted as the organization of the amorphous polymers.[48] P values were obtained in the 2.0−2.2 range, which indicates that amorphous cell wall polymers, lignin and hemicellulose, exhibit a randomly flexible conformation that remains the same as the QsuB expression level is increased. Similarly, SAXS analysis of WT shows that the scattering intensity decreases as the delignification reaction progresses (Figure S6). Furthermore, the P values obtained in the Level 3 region, like that observed in the equatorial sector, are ∼4.0 and indicate a smooth surface of the large structures.

WAXS Data Analysis. Intact stem sections of WT and the QsuB transgenic lines produced distinctly different 2D WAXS patterns, as shown in Figure 4. There are two important trends. First, the overall WAXS intensity decreased with increasing

QsuB expression. Second, the images showed a progressively increased split in the scattering intensity peak in the equatorial direction, indicating the emergence of two coexisting orientations of the microfibrils within the plant cell wall that increases with the QsuB expression level.

For analysis, the Q_y vs Q_x 2D plots shown in Figure 4 were transformed to polar plots Q vs azimuthal angle (ϕ). The data for WT and QsuB1 are shown in Figure 5, while the data for

Figure 5. Two-dimensional WAXS scattering data are shown in two representations—as Q_y vs. Q_x and Q vs. ϕ plots for WT (A and C) and QsuB1 (B and D) samples, respectively.

Qsu5 and Qsu15 are shown in the Supporting Information (Figure S9). The Q vs ϕ for WT and QsuB1 (Figure 5C,D) showed intense scattering regions that represent the crystalline reflections of the cellulose microfibril, as indicated by boxes F, G, and H. The $1\bar{1}0$/110 (box F), 200 (box G), and 004 (box H) crystalline reflections of cellulose I were plotted in the ϕ-profile panels of Figure 6 with labels F−H, respectively. The polar images and ϕ-profiles of WT and QsuB1 transgenic line showed clear differences. A split in the peaks was observed for every crystalline reflection of QsuB1. 1D WAXS patterns were generated by averaging over the range of azimuthal angles (Figure 6 panels J, K, and L). These patterns were analyzed to determine the structure of the crystallites. The ϕ-profiles in Figure 6 allow the details of the orientation angle of the
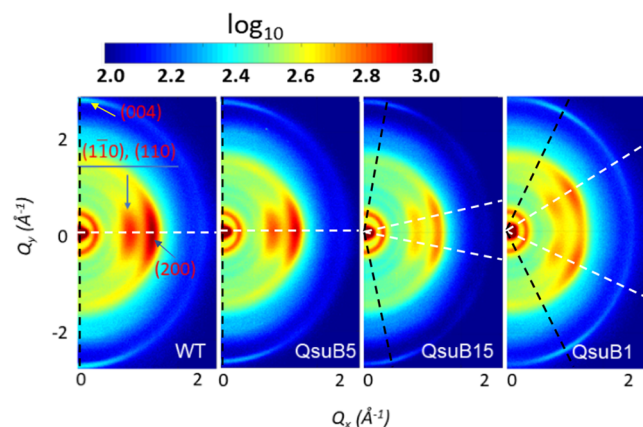

Figure 4. Two-dimensional WAXS images of poplar samples with increasing QsuB expression—WT, QsuB5, QsuB15, and QsuB1. The white line represents the change in (110, $1\bar{1}0$) and (200) diffraction angles, while the black line represents the shift in (004) reflection with increasing QsuB expression level. Only the right half of the diffraction images are shown. The diffraction intensity scale is shown on a log scale.
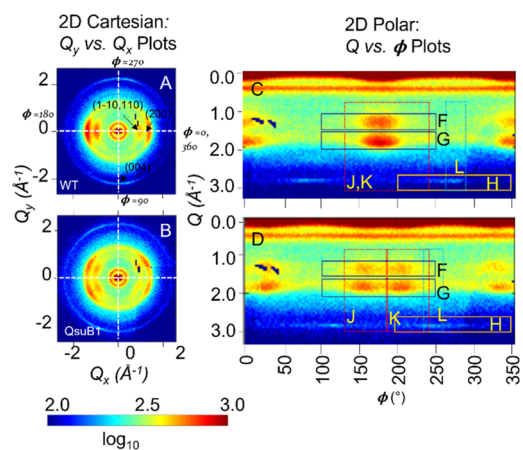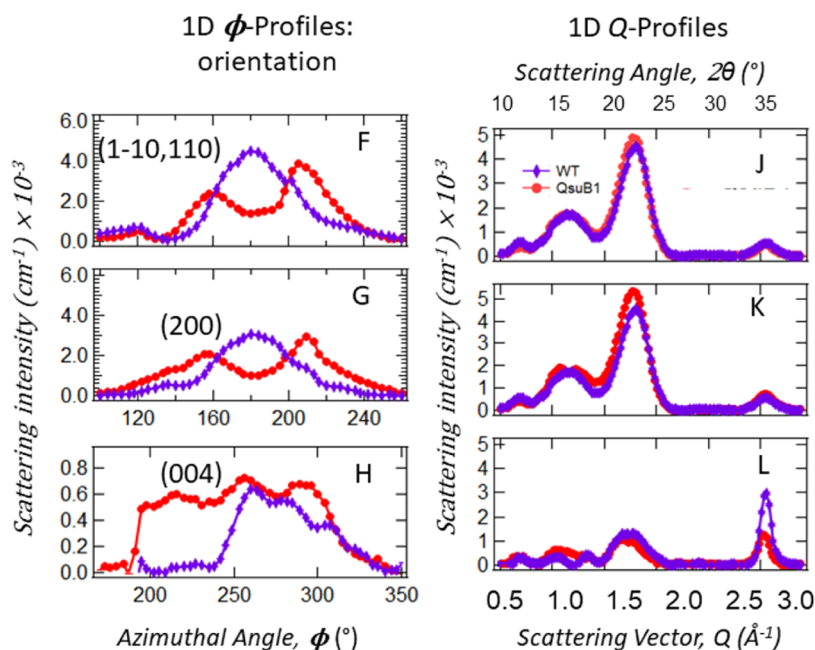
Figure 6. (F−H) One-dimensional ϕ-profiles define cellulose microfibril orientation from the scattering intensity vs. azimuthal angle ϕ plots of cellulose I reflections—1$\bar{1}$0/110 (F), 200 (G), and 004 (H) averaged over Q as illustrated in F, G, and H boxes in Figure 5. Plots F and G are made after linear subtraction of background scattering to match the baseline. One-dimensional WAXS data after subtraction of the amorphous contribution are shown as Q profiles for different ϕ ranges as illustrated in J, K, and L boxes in Figure 5C,D. All the plots compare patterns between WT (purple) and QsuB1 transgenic lines (red).

cellulose microfibril axis in relation to the growth axis of the plant stem to be observed.

The peaks in the ϕ-profiles were fit to Gaussian functions (illustrated in Figure S11) to obtain the peak center and FWHM parameters, which is a quantitative measure of the microfibril central orientation angle and distribution about that central angle. The WT (Figure 6, purple diamonds in panels F and G) and QsuB5 (Figure S10, green squares in panels F and G) were fit with one Gaussian function to obtain the orientation angle at 183°, which is parallel to the growth direction of the plant stem. On the other hand, the QsuB15 (Figure S10, blue triangles in panels F and G) and QsuB1 mutants showed split peaks (Figure 6, red circles in panels F−G) and, therefore, required two Gaussian functions to fit the data. This resulted in two orientation angles centered at 177° (difference of −6°) and 203° (+13°) for QsuB15 and at 156° (difference of −26°) and 208° (+24°) for QsuB1, almost symmetrically deviating from the growth direction of 183°. The scattering intensity of the 156° oriented microfibrils is consistently lower compared to the 207° oriented microfibrils for 1$\bar{1}$0/110 and 200 reflections of Cellulose I. This implies that more cellulose microfibrils are oriented at 207° than at 153°. The Gaussian function fits of ϕ-profiles of WT and transgenic lines for (1$\bar{1}$0/110) and (200) diffraction planes are illustrated in Figure S11. The ϕ-profile of (004) reflection plane shows split peaks (Figure 6, panel H) in WT, while QsuB1 results in a very broad split peak. This observation can be attributed to the twisting of microfibrils at different angles along the fiber axis.[49]

The Q profiles were further analyzed to calculate the percent cellulose crystallinity and crystal width, as described in the Materials and Methods section. The (1$\bar{1}$0/110) and (200) diffraction peaks were fitted with three Gaussian peaks (see the Figure S12A−E), and the (004) diffraction peaks were fitted with a single PseudoVoigt function (see Figure S13A−D) to

extract the crystalline peak area, full width at half maxima of the peaks (FWHM), and the peak positions. These values were then used to calculate the crystallite size and the crystallinity of the systems as described in the Materials and Methods section. The results for the WT and QsuB lines are summarized in Table 3. The crystallite sizes of WT and QsuB lines in the

Table 3. Crystallite Size and Percent Crystallinity of WT and QsuB1 Transgenic Lines

	crystallite size (Å)				crystallinity (%)[a]
	J, K profiles			L profile	J, K, L profiles
sample	(1$\bar{1}$0)	(110)	(200)	(004)	
WT 183°	28 ± 1	28 ± 1	29 ± 2	84 ± 1	60 ± 2
QsuB5 183°	28 ± 1	28 ± 1	30 ± 2	79 ± 3	59 ± 1
QsuB15 177°	27 ± 1	28 ± 1	29 ± 1	74 ± 1	56 ± 2
QsuB15 203°	28 ± 1	27 ± 1	28 ± 1		54 ± 1
QsuB1 156°	26 ± 2	27 ± 1	28 ± 1	67 ± 2	55 ± 1
QsuB1 208°	27 ± 2	27 ± 2	28 ± 2		53 ± 1

[a]%Crystallinity is the sum of areas under (1$\bar{1}$0), (110), and (200) peaks divided by total area.

(110), (1$\bar{1}$0), and (200) diffraction planes perpendicular to the fiber axis are approximately ∼28 Å. Similar crystallite sizes in WT and QsuB lines in the perpendicular planes show that the crystallite size is not affected by the QsuB expression level. This is consistent with the SANS data that shows no effect of QsuB expression on the cross-sectional dimensions of the cellulose microfibrils. The peak position of the (004) plane was 34.6° for WT and QsuB lines, which corresponds to ∼2.25 Å ($2d \sin \theta = n\lambda$) between two consecutive planes along the growth direction. The crystallite size obtained was ∼60 Å for WT, which corresponds to 26 (60/2.25) consecutive planes in

the growth direction (see Figure S14). However, the crystallite size in the (004) plane decreased in the QsuB lines (Table 3) and was ∼20% smaller in QsuB1 compared to WT. The cellulose crystallinity was estimated for the WT and the transgenic lines as the ratio of the area of the crystalline peaks to the amorphous background for each of the scattering orientations observed in the 2D scattering profiles. The data show a significant decrease in cellulose crystallinity with increasing QsuB expression, with the highest expressing line, QsuB1, showing ∼11% reduction in crystalline cellulose compared to the WT.

Effect of DHBA on Cellulose Formation in Bacteria. Based on the WAXS results that show a decrease in cellulose crystallinity in the transgenic poplar with increased QsuB expression, we tested the effect of DHBA on cellulose production by *Acetobacter sp.* This bacteria has been previously used as a model system for studying cellulose synthesis and has the advantage of being produced in a relatively pure state without interfering contribution from the matrix copolymers found in plants.[50] In this study, *Acetobacter xylinum sp. sucrofermentan* cultures were grown in the presence of different concentrations of DHBA (0−100 μM). After harvesting and cleaning the cellulose pellicles that formed on the surface of the cultures, the cellulose was analyzed by WAXS using the same approach described for the transgenic poplar (Figure S15). The results show a decrease in cellulose crystallinity with increasing DHBA concentration similar to the effect that was observed in the transgenic poplar lines (Figure 7).
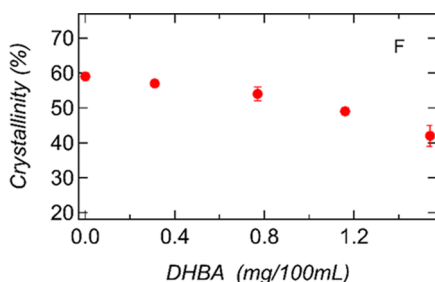

Figure 7. Cellulose crystallinity of bacterial cellulose synthesized in the presence of dihydroxybenzoic acid (DHBA) in the growth medium. Plot shows cellulose crystallinity (%) versus DHBA concentration (0, 0.31, 0.77, 1.16, and 1.54 mg/100 mL DHBA) determined by WAXS.

■ DISCUSSION

Our overall aim was to investigate a structural basis for the observed increase in saccharification of poplar QsuB transgenic trees.[33,37] These lines are characterized by a reduction in lignin deposition that is correlated with increased production of DHBA.[33] Additionally, a concomitant increase in xylan, albeit at lower amounts, was also observed in the transgenic plants.[33]

SANS showed that the cellulose microfibril cross section of WT is ∼20 Å, which agrees well with the previously reported values in similar studies,[51,52] and is consistent with the 18 cellulose chain model for a microfibril.[53,54] In addition, we did not observe differences in the microfibril cross-sectional dimensions of the transgenic lines, supporting that QsuB expression did not affect the formation of the cellulose microfibrils. The intermicrofibril distance of WT poplar is ∼30 Å and agrees with the values reported in previous studies.[52,54,55] However, the intermicrofibril distance pro-

gressively increased as the QsuB expression level was increased. In addition, the orientation and packing of the microfibrils relative to each other also decreased, indicating that there was increased disorder in their arrangement. No correlations between microfibrils were observed in the highest expressing QsuB line, suggesting that the cellulose organization in this tree was severely impaired. Decreased order in cellulose microfibril organization was previously observed in naturally occurring poplar variants and was attributed to a decrease in lignin content in the secondary cell walls.[55] In addition, changes in cellulose microfibril organization have also been observed previously when the matrix copolymers, lignin and hemicellulose, are either redistributed or removed during biomass thermochemical pretreatment.[56,57] The aggregation or removal of lignin and hemicellulose allows increased interactions between cellulose microfibrils by exposing cellulose surfaces that can form hydrogen bonds between the adjacent microfibrils allowing them to coalesce to form aggregated microfibrils.[58] However, in the case of mutant plants with decreased lignin, the situation is likely different. Our current view of the plant cell wall is that the cellulose microfibrils and hemicelluloses interact together to form macrofibrils. Hemicelluloses such as xylan interact directly with cellulose by cocrystallization of xylan with cellulose,[59] through the formation of strong xylan-cellulose hydrogen interactions.[60] The lignin is deposited around the macrofibrils and primarily interacts with hemicellulose through weak noncovalent bonding,[61] and possibly covalent lignin−carbohydrate bonds[62] formed via α-ether[63] and γ-ester bonds.[64,65] Decreased lignin content reduces the number of H-bonding interactions, while increased hemicellulose content could increase the steric hindrance between microfibrils. Both can affect microfibril organization and can account for a larger center-to-center distance with increasing QsuB expression levels. Overall, we can infer that the decreased lignin deposition means that there are fewer constraints on the assembly of the macrofibrils during the formation of the secondary cell walls that may allow cellulose macrofibrils to become increasingly unordered. This supports an important role for lignin in guiding the assembly and organization of the cellulose microfibrils in plant cell walls and maintaining the organization in established cell walls.

In our SANS analysis approach, we analyzed different sectors of the 2D detector images to resolve the scattering signatures of the cellulose microfibrils aligned along the growth direction of the trees (equatorial sector) from the other components of the cell wall (meridional sector). The meridional sector mainly captures the structural characteristics of the amorphous polymers because they are randomly distributed producing an isotropic scattering signature. However, we observed a feature in the high-Q region ($Q > 0.1$ Å^{-1}) that we interpreted as cellulose microfibrils aligned perpendicular to the growth direction.[66,67] The apparent increased radius of the microfibrils is most probably related to the misalignment of cellulose microfibrils relative to each other as the QsuB expression level increased, similar to the changes observed for the cellulose microfibrils oriented along plant growth direction. Interestingly, we did not observe any significant change in the mid-Q scattering region ($0.01 < Q < 0.1$ Å^{-1}), which is sensitive to the organization of lignin and hemicellulose in the cell walls.[57] This was also observed in a GAUT4-KD switchgrass mutant, which has reduced pectin, but no significant change in the distribution of the copolymer matrix.[68] The power-law

exponent, ~2 in all cases, is interpreted as random polymer chains[69] and is similar to ones previously reported using SANS[57] and molecular dynamics simulations.[70] This suggests that although the composition and amount of lignin and hemicelluloses have changed, their overall organization and distribution have not, at least on the length scales (~1−600 nm) observed in this experiment.

Significant changes were also observed in the crystalline structure of the QsuB transgenic lines compared to WT. A bimodal distribution of the cellulose microfibrils was observed as the QsuB expression level increased. This is interpreted as helical twisting[49] of the microfibrils at different angles along the growth orientation of the trees. A similar distribution of cellulose fibers in intact primary cell walls has been observed previously using different imaging modalities including cryo-electron tomography and atomic force microscopy.[71,72] Although the reason for the transition from a unimodal distribution in WT to the appearance of a bimodal distribution in the orientation of cellulose microfibrils is unclear, the fact is that it correlated with a reduction in the lignin content, and a change in its molecular weight distribution suggests that the cellulose macrofibrils may be less restrained in the apoplastic space allowing them to adopt an alternative orientation. It is of interest to note that the integrity of the stems was reduced with increasing QsuB expression with the transgenic lines being susceptible to splitting along the length of the growth axis, consistent with the findings of reduced crystallite size along the stem axis (004 plane), indicating that the QsuB trees display a lignocellulose architecture that is likely less stable than WT trees.[33]

The overall cellulose crystalline content was reduced in the transgenic plants by approximately 10% in the highest DHBA containing line. This was somewhat unexpected because in previous characterization of native poplar with decreased lignin, an increase in cellulose crystallinity was observed.[55] In addition, increased crystalline cellulose content was also observed in thermochemically pretreated plants, in which lignin removal and redistribution were evident.[56,72] The increased cellulose crystallinity after pretreatment is attributed to coalescence of adjacent microfibrils that facilitates more hydrogen bonding between adjacent cellulose chains. A closer examination of cellulose microfibril structure showed that the dimensions of the crystalline planes transverse to the growth direction (100), (1$\bar{1}$0), and (200) were unchanged with increasing QsuB expression compared to WT trees. The dimensions of these planes are determined by the combination of a number of cellulose chains in the fibril, cross-sectional shape, degree of order in the packing of cellulose chains, and heterogeneity of crystal lattice constant.[73] The similar crystal dimensions in transverse planes show that QsuB expression does not affect the number of cellulose chains and their intrinsic order within a microfibril. However, the crystallite dimension in the (004) diffraction plane that is parallel to the growth direction of the trees progressively decreased with increased QsuB expression (see Figure S14). This can be attributed to the defects such as twisting of the microfibril that result in the loss of axial coherence, which has previously been observed.[49,73]

However, this does not account for the decreased cellulose crystalline content that was observed in the current study. Based on previous reported work, it is unlikely that the changes in the overall amount and composition of the lignin observed in the QsuB trees could account for the observed decreased

crystallinity of the cellulose. Unda et al.[33] previously reported that ~7.1−11.6 mg/g^{-1} accumulation of DHBA in the transgenic cell walls compared to no DHBA is detected in WT trees. Based on this, we hypothesized that DHBA itself may play a role in decreasing the cellulose crystallinity. It is well-established that the addition of chemical additives to cellulose producing *Acetobacter* cultures can decrease the crystallinity of the secreted cellulose. A recent study investigated the effects of addition of dye molecules during bacterial growth on bacterial cellulose crystallinity.[74] Although the dyes tested had a significantly more complex molecular architecture compared to DHBA, the distinguishing feature of the molecule that was most effective in decreasing cellulose crystallinity, brilliant yellow, was that it had terminal phenolic groups reminiscent of DHBA (see Figure S16). We tested the effect of DHBA on cellulose produced by *A. xylinum* subsp. *sucrofermentans* and showed a concomitant decrease in cellulose crystallinity compared to the control culture. This supports our hypothesis that production of DHBA during cell wall synthesis can directly affect cellulose microfibril structure. Therefore, we propose that the disruption of native cellulose microfibril structure by incorporation of DHBA could play a significant role in the increased saccharification observed in these transgenic lines beyond the impact of decreased lignin content and the changes in its composition. We recognize that there are drawbacks with using bacterial cellulose as a model for plant cellulose. These include a different microfibril structure,[75] the major cellulose crystal allomorph is cellulose 1α rather than cellulose 1β in plants,[76,77] and cellulose synthesis and assembly of the microfibrils in bacterial cultures occur in the absence of the matrix copolymers found in plants.[50] Additional analysis of cellulose structure *in planta* or in a model system is needed to verify if DHBA is in fact incorporated into cellulose microfibrils in plants.

■ CONCLUSIONS

Genetic engineering has transformed our ability to modify plant cell walls to optimize their properties for applications in bioenergy, biochemicals, and biomaterials. The QsuB trees characterized in this study were modified by introducing a bacterial 3-dehydroshikimate dehydratase to divert carbon flux away from the shikimate pathway. This significantly reduced the total lignin content, resulting in the accumulation of DHBA and its glycoside derivatives and the production of a newly engineered zip-lignin polymer.[33] In this study, we show that 3-dehydroshikimate dehydratase expression also significantly disrupts cellulose organization that is correlated with decreased lignin content and possible decreased mechanical strength of the plants. In addition, we show that cellulose structure is also affected by DHBA levels providing evidence that it can disrupt cellulose microfibril crystallization by its incorporation between the cellulose chains. Although it is well-established that small molecules can disrupt cellulose synthesis in bacterial cell cultures, based on the work presented here, we can propose that this can also manifest in plant cell walls. This presents a new strategy to consider for altering plant cell wall properties to decrease their recalcitrance by producing small-molecule metabolites that interfere with cellulose microfibril crystallization to increase their susceptibility to chemical or biochemical degradation.

ASSOCIATED CONTENT

SI **Supporting Information**

The Supporting Information is available free of charge at https://pubs.acs.org/doi/10.1021/acs.biomac.4c00187.

Comparison of WT and poplar transgenic stems, wedge reduction of SANS and SAXS data, unscaled 1D meridional and equatorial SANS data and approach for wedge reduction of SANS and SAXS data, delignification procedure and SAXS analysis of delignified poplar stems, illustration of cellulose microfibrils in meridional direction, WAXS data analysis of QsuB5 and QsuB15 poplar stems, biosynthesis of bacterial cellulose synthesis with DHBA and WAXS characterization, DHBA structure, and brilliant yellow structures (PDF)

AUTHOR INFORMATION

Corresponding Authors

Sai Venkatesh Pingali — *Neutron Scattering Division, Oak Ridge National Laboratory, Oak Ridge, Tennessee 37831, United States;* ⊙ orcid.org/0000-0001-7961-4176; Email: pingalis@ornl.gov

Hugh O'Neill — *Neutron Scattering Division, Oak Ridge National Laboratory, Oak Ridge, Tennessee 37831, United States;* ⊙ orcid.org/0000-0003-2966-5527; Email: oneillhm@ornl.gov

Authors

Manjula Senanayake — *Neutron Scattering Division, Oak Ridge National Laboratory, Oak Ridge, Tennessee 37831, United States;* ⊙ orcid.org/0000-0002-3139-0625

Chien-Yuan Lin — *Joint BioEnergy Institute, Emeryville, California 94608, United States; Environmental Genomics and Systems Biology Division, Lawrence Berkeley National Laboratory, Berkeley, California 94720, United States*

Shawn D. Mansfield — *Department of Wood Science and Department of Botany, University of British Columbia, Vancouver, BC V6T 1Z4, Canada*

Aymerick Eudes — *Joint BioEnergy Institute, Emeryville, California 94608, United States; Environmental Genomics and Systems Biology Division, Lawrence Berkeley National Laboratory, Berkeley, California 94720, United States;* ⊙ orcid.org/0000-0002-1387-6111

Brian H. Davison — *BioSciences Division, Oak Ridge National Laboratory, Oak Ridge, Tennessee 37831, United States;* ⊙ orcid.org/0000-0002-7408-3609

Complete contact information is available at: https://pubs.acs.org/10.1021/acs.biomac.4c00187

Author Contributions

M.S. prepared samples for analysis, performed small-angle scattering (SAS), and diffraction experiments and data analysis. C.-Y.L., S.D.M., and A.E. provided samples for characterization. S.V.P. directed SAS and WAXS measurements. H.O'N. and S.V.P. directed the research. M.S., S.V.P., and H.O'N. wrote the manuscript with input from all coauthors. All authors had the opportunity to read and comment on the manuscript.

Notes

The authors declare no competing financial interest.

ACKNOWLEDGMENTS

REFERENCES

(1) Ray, S.; Abraham, J.; Jordan, N.; Lindsay, M.; Chauhan, N. Synthetic, Photosynthetic, and Chemical Strategies to Enhance Carbon Dioxide Fixation. *C* **2022**, *8*, 18.

(2) Cosgrove, D. J. Growth of the Plant Cell Wall. *Nat. Rev. Mol. Cell Biol.* **2005**, *6*, 850−861.

(3) Meents, M. J.; Watanabe, Y.; Samuels, A. L. The Cell Biology of Secondary Cell Wall Biosynthesis. *Ann. Bot.* **2018**, *121*, 1107−1125.

(4) Dahmen, N.; Lewandowski, I.; Zibek, S.; Weidtmann, A. Integrated Lignocellulosic Value Chains in a Growing Bioeconomy: Status Quo and Perspectives. *GCB Bioenergy* **2019**, *11*, 107−117.

(5) Rodionova, M. V.; Poudyal, R. S.; Tiwari, I.; Voloshin, R. A.; Zharmukhamedov, S. K.; Nam, H. G.; Zayadan, B. K.; Bruce, B. D.; Hou, H. J.; Allakhverdiev, S. I. Biofuel Production: Challenges and Opportunities. *Int. J. Hydrogen Energy* **2017**, *42*, 8450−8461.

(6) Neuling, U.; Kaltschmitt, M. Review of Biofuel Production-Feedstock, Processes and Markets − Review Article. *J. Oil Palm Res.* **2017**, *29*, 137−167.

(7) Malode, S. J.; Prabhu, K. K.; Mascarenhas, R. J.; Shetti, N. P.; Aminabhavi, T. M. Recent Advances and Viability in Biofuel Production. *Energy Convers. Manage.: X* **2021**, *10*, No. 100070.

(8) Balasundaram, G.; Banu, R.; Varjani, S.; Kazmi, A. A.; Tyagi, V. K. Recalcitrant Compounds Formation, Their Toxicity, and Mitigation: Key Issues in Biomass Pretreatment and Anaerobic Digestion. *Chemosphere* **2022**, *291*, No. 132930.

(9) Melati, R. B.; Shimizu, F. L.; Oliveira, G.; Pagnocca, F. C.; de Souza, W.; Sant'Anna, C.; Brienzo, M. Key Factors Affecting the Recalcitrance and Conversion Process of Biomass. *BioEnergy Res.* **2019**, *12*, 1−20.

(10) Lynd, L. R.; Wyman, C. E.; Gerngross, T. U. Biocommodity Engineering. *Biotechnol. Prog.* **1999**, *15*, 777−793.

(11) Bajpai, P. Structure of Lignocellulosic Biomass. In *Pretreatment of Lignocellulosic Biomass for Biofuel Production*; Springer: Singapore, 2016; pp 7−12.

(12) Ashokkumar, V.; Venkatkarthick, R.; Jayashree, S.; Chuetor, S.; Dharmaraj, S.; Kumar, G.; Chen, W.-H.; Ngamcharussrivichai, C. Recent Advances in Lignocellulosic Biomass for Biofuels and Value-Added Bioproducts - A Critical Review. *Bioresour. Technol.* **2022**, *344*, 126195−126210.

(13) Österberg, M.; Sipponen, M. H.; Henriksson, G. From Understanding the Biological Function of Lignin in Plants to Production of Colloidal Lignin Particles. *Nordic Pulp Paper Res. J.* **2017**, *32*, 483−484.

(14) Mottiar, Y.; Vanholme, R.; Boerjan, W.; Ralph, J.; Mansfield, S. D. Designer Lignins: Harnessing the Plasticity of Lignification. *Curr. Opin. Biotechnol.* **2016**, *37*, 190−200.

(15) Studer, M. H.; DeMartini, J. D.; Davis, M. F.; Sykes, R. W.; Davison, B.; Keller, M.; Tuskan, G. A.; Wyman, C. E. Lignin Content in Natural Populus Variants Affects Sugar Release. *Proc. Natl. Acad. Sci. U.S.A.* **2011**, *108*, 6300−6305.

(16) Porth, I.; Klápště, J.; Skyba, O.; Lai, B. S.; Geraldes, A.; Muchero, W.; Tuskan, G. A.; Douglas, C. J.; El-Kassaby, Y. A.; Mansfield, S. D. Populus trichocarpa Cell Wall Chemistry and Ultrastructure Trait Variation, Genetic Control and Genetic Correlations. *New Phytol.* **2013**, *197*, 777−790.

(17) Li, M.; Pu, Y.; Ragauskas, A. J. Current Understanding of the Correlation of Lignin Structure with Biomass Recalcitrance. *Front. Chem.* **2016**, *4*, 45.

(18) Yoo, C. G.; Dumitrache, A.; Muchero, W.; Natzke, J.; Akinosho, H.; Li, M.; Sykes, R. W.; Brown, S. D.; Davison, B.; Tuskan, G. A.; Pu, Y.; Ragauskas, A. J. Significance of Lignin S/G Ratio in Biomass Recalcitrance of Populus trichocarpa Variants for Bioethanol Production. *ACS Sustainable Chem. Eng.* **2018**, *6*, 2162−2168.

(19) Stewart, J. J.; Akiyama, T.; Chapple, C.; Ralph, J.; Mansfield, S. D. The Effects on Lignin Structure of Overexpression of Ferulate 5-Hydroxylase in Hybrid Poplar. *Plant Physiol.* **2009**, *150*, 621−635.

(20) Dumitrache, A.; Akinosho, H.; Rodriguez, M.; Meng, X.; Yoo, C. G.; Natzke, J.; Engle, N. L.; Sykes, R. W.; Tschaplinski, T. J.; Muchero, W.; Ragauskas, A. J.; Davison, B. H.; Brown, S. D. Consolidated Bioprocessing of Populus using Clostridium (Ruminiclostridium) thermocellum: A Case Study on the Impact of Lignin Composition and Structure. *Biotechnol. Biofuels* **2016**, *9*, No. 31.

(21) Mansfield, S. D.; Kang, K. Y.; Chapple, C. Designed for deconstruction−poplar trees altered in cell wall lignification improve the efficacy of bioethanol production. *New Phytol.* **2012**, *194*, 91−101.

(22) Mankar, A. R.; Pandey, A.; Modak, A.; Pant, K. Pretreatment of lignocellulosic biomass: A review on recent advances. *Bioresour. Technol.* **2021**, *334*, 125235−125247.

(23) Liu, W.-J.; Yu, H.-Q. Thermochemical Conversion of Lignocellulosic Biomass into Mass-Producible Fuels: Emerging Technology Progress and Environmental Sustainability Evaluation. *ACS Environ. Au* **2022**, *2*, 98−114.

(24) Balan, V. Current Challenges in Commercially Producing Biofuels from Lignocellulosic Biomass. *ISRN Biotechnol.* **2014**, *2014*, 1−32.

(25) Baudel, H. M.; Rodrigues, D. M.; Diebold, E.; Chandel, A. K. Scale-up Process Challenges in Lignocellulosic Biomass Conversion and Possible Solutions to Overcome the Hurdles. In *Lignocellulose Bioconversion Through White Biotechnol.*; Wiley Online Library, 2022; pp 289−311.

(26) Li, X.; Weng, J. K.; Chapple, C. Improvement of biomass through lignin modification. *Plant J.* **2008**, *54*, 569−581.

(27) Fraser, C. M.; Chapple, C. The phenylpropanoid pathway in Arabidopsis. *Arabidopsis Book* **2011**, *9*, No. e0152.

(28) Herrmann, K. M.; Weaver, L. M. The shikimate pathway. *Annu. Rev. Plant Physiol. Plant Mol. Biol.* **1999**, *50*, 473−503.

(29) Whetten, R.; Sederoff, R. Lignin Biosynthesis. *Plant Cell* **1995**, *7*, 1001−1013.

(30) Eudes, A.; Sathitsuksanoh, N.; Baidoo, E. E.; George, A.; Liang, Y.; Yang, F.; Singh, S.; Keasling, J. D.; Simmons, B. A.; Loqué, D. Expression of a bacterial 3-dehydroshikimate dehydratase reduces lignin content and improves biomass saccharification efficiency. *Plant Biotechnol. J.* **2015**, *13*, 1241−1250.

(31) Hu, S.; Kamimura, N.; Sakamoto, S.; Nagano, S.; Takata, N.; Liu, S.; Goeminne, G.; Vanholme, R.; Uesugi, M.; Yamamoto, M.; et al. Rerouting of the lignin biosynthetic pathway by inhibition of cytosolic shikimate recycling in transgenic hybrid aspen. *Plant J.* **2022**, *110*, 358−376.

(32) Eudes, A.; Pereira, J. H.; Yogiswara, S.; Wang, G.; Teixeira Benites, V.; Baidoo, E. E.; Lee, T. S.; Adams, P. D.; Keasling, J. D.; Loqué, D. Exploiting the substrate promiscuity of hydroxycinnamoyl-CoA: shikimate hydroxycinnamoyl transferase to reduce lignin. *Plant Cell Physiol.* **2016**, *57*, 568−579.

(33) Unda, F.; Mottiar, Y.; Mahon, E. L.; Karlen, S. D.; Kim, K. H.; Loqué, D.; Eudes, A.; Ralph, J.; Mansfield, S. D. A new approach to zip-lignin: 3,4-dihydroxybenzoate is compatible with lignification. *New Phytol.* **2022**, *235*, 234−246.

(34) Himmel, M. E.; Ding, S.-Y.; Johnson, D. K.; Adney, W. S.; Nimlos, M. R.; Brady, J. W.; Foust, T. D. Biomass recalcitrance: engineering plants and enzymes for biofuels production. *Science* **2007**, *315*, 804−807.

(35) Langan, P.; Petridis, L.; O'Neill, H. M.; Pingali, S. V.; Foston, M.; Nishiyama, Y.; Schulz, R.; Lindner, B.; Hanson, B. L.; Harton, S.; et al. Common processes drive the thermochemical pretreatment of lignocellulosic biomass. *Green Chem.* **2014**, *16*, 63−68.

(36) Donohoe, B. S.; Decker, S. R.; Tucker, M. P.; Himmel, M. E.; Vinzant, T. B. Visualizing lignin coalescence and migration through maize cell walls following thermochemical pretreatment. *Biotechnol. Bioeng.* **2008**, *101*, 913−925.

(37) Lin, C.-Y.; Geiselman, G. M.; Liu, D.; Magurudeniya, H. D.; Rodriguez, A.; Chen, Y.-C.; Pidatala, V.; Unda, F.; Amer, B.; Baidoo, E. E.; et al. Evaluation of engineered low-lignin poplar for conversion into advanced bioproducts. *Biotechnol. Biofuels Bioprod.* **2022**, *15*, No. 145.

(38) Ilavsky, J.; Jemian, P. R. Irena: tool suite for modeling and analysis of small-angle scattering. *J. Appl. Crystallogr.* **2009**, *42*, 347−353.

(39) Mark, J.; Lee, C.; Bianconi, P. *Hybrid Organic-Inorganic Composites*; ACS Symposium Series, Bianconi, P. A., Ed.; ACS Publications, 1994; pp 97−111.

(40) Weisstein, E. W., Least squares fitting. https://mathworld.wolfram.com, 2002 (accessed 2022−04−20).

(41) Wojdyr, M. Fityk: a general-purpose peak fitting program. *J. Appl. Crystallogr.* **2010**, *43*, 1126−1128.

(42) Langford, J. I.; Wilson, A. Scherrer after sixty years: a survey and some new results in the determination of crystallite size. *J. Appl. Crystallogr.* **1978**, *11*, 102−113.

(43) Valla, S.; Kjosbakken, J. Isolation and characterization of a new extracellular polysaccharide from a cellulose-negative strain of *Acetobacter xylinum*. *Can. J. Microbiol.* **1981**, *27*, 599−603.

(44) Su, Y.; Burger, C.; Ma, H.; Chu, B.; Hsiao, B. S. Exploring the nature of cellulose microfibrils. *Biomacromolecules* **2015**, *16*, 1201−1209.

(45) Pingali, S. V.; Urban, V. S.; Heller, W. T.; McGaughey, J.; O'Neill, H. M.; Foston, M.; Myles, D. A.; Ragauskas, A. J.; Evans, B. R. SANS study of cellulose extracted from switchgrass. *Acta Crystallogr., Sect. D: Biol. Crystallogr.* **2010**, *66*, 1189−1193.

(46) Shah, R.; Huang, S.; Pingali, S. V.; Sawada, D.; Pu, Y.; Rodriguez, M., Jr; Ragauskas, A. J.; Kim, S. H.; Evans, B. R.; Davison, B. H.; O'Neill, H. Hemicellulose−cellulose composites reveal differences in cellulose organization after dilute acid pretreatment. *Biomacromolecules* **2019**, *20*, 893−903.

(47) Plaza, N. Z.; Pingali, S. V.; Qian, S.; Heller, W. T.; Jakes, J. E. Informing the improvement of forest products durability using small angle neutron scattering. *Cellulose* **2016**, *23*, 1593−1607.

(48) Pingali, S. V.; Urban, V. S.; Heller, W. T.; McGaughey, J.; O'Neill, H.; Foston, M. B.; Li, H.; Wyman, C. E.; Myles, D. A.;

Langan, P.; Ragauskas, A.; Davison, B.; Evans, B. R. Understanding Multiscale Structural Changes During Dilute Acid Pretreatment of Switchgrass and Poplar. *ACS Sustainable Chem. Eng.* **2017**, *5*, 426−435.

(49) Emons, A. M. C.; Mulder, B. M. The making of the architecture of the plant cell wall: how cells exploit geometry. *Proc. Natl. Acad. Sci. U.S.A.* **1998**, *95*, 7215−7219.

(50) Brown, R. M., Jr. The biosynthesis of cellulose. *J. Macromol. Sci., Part A: Pure Appl. Chem.* **1996**, *33*, 1345−1373.

(51) Thomas, L. H.; Forsyth, V. T.; Šturcová, A.; Kennedy, C. J.; May, R. P.; Altaner, C. M.; Apperley, D. C.; Wess, T. J.; Jarvis, M. C. Structure of cellulose microfibrils in primary cell walls from collenchyma. *Plant Physiol.* **2012**, *161*, 465−476.

(52) Sawada, D.; Kalluri, U. C.; O'Neill, H.; Urban, V.; Langan, P.; Davison, B.; Pingali, S. V. Tension wood structure and morphology conducive for better enzymatic digestion. *Biotechnol. Biofuels* **2018**, *11*, No. 44.

(53) Hill, J. L., Jr.; Hammudi, M. B.; Tien, M. The Arabidopsis Cellulose Synthase Complex: A Proposed Hexamer of CESA Trimers in an Equimolar Stoichiometry. *Plant Cell* **2015**, *26* (12), 4834−4842.

(54) Kubicki, J. D.; Yang, H.; Sawada, D.; O'Neill, H.; Oehme, D.; Cosgrove, D. The Shape of Native Plant Cellulose Microfibrils. *Sci. Rep.* **2018**, *8*, No. 13983.

(55) Shah, R.; Bhagia, S.; Keum, J. K.; Pingali, S. V.; Ragauskas, A. J.; Davison, B. H.; O'Neill, H. Structural insights into low and high recalcitrance natural poplar variants using neutron and X-ray scattering. *ACS Sustainable Chem. Eng.* **2020**, *8*, 13838−13849.

(56) Lancha, J. P.; Perré, P.; Colin, J.; Lv, P.; Ruscassier, N.; Almeida, G. Multiscale investigation on the chemical and anatomical changes of lignocellulosic biomass for different severities of hydrothermal treatment. *Sci. Rep.* **2021**, *11*, No. 8444.

(57) Pingali, S. V.; Urban, V. S.; Heller, W. T.; McGaughey, J.; O'Neill, H.; Foston, M.; Myles, D. A.; Ragauskas, A.; Evans, B. R. Breakdown of cell wall nanostructure in dilute acid pretreated biomass. *Biomacromolecules* **2010**, *11*, 2329−2335.

(58) Sun, Q.; Foston, M.; Meng, X.; Sawada, D.; Pingali, S. V.; O'Neill, H. M.; Li, H.; Wyman, C. E.; Langan, P.; Ragauskas, A. J.; Kumar, R. Effect of lignin content on changes occurring in poplar cellulose ultrastructure during dilute acid pretreatment. *Biotechnol. Biofuels* **2014**, *7*, No. 150.

(59) Linder, Å.; Bergman, R.; Bodin, A.; Gatenholm, P. Mechanism of assembly of xylan onto cellulose surfaces. *Langmuir* **2003**, *19*, 5072−5077.

(60) Mora, F.; Ruel, K.; Comtat, J.; Joseleau, J.-P. Aspect of native and redeposited xylans at the surface of cellulose microfibrils. *Holzforschung* **1986**, *40*, 85−91.

(61) Jarvis, M. C. Hydrogen bonding and other non-covalent interactions at the surfaces of cellulose microfibrils. *Cellulose* **2023**, *30*, 667−687.

(62) Terrett, O. M.; Dupree, P. Covalent interactions between lignin and hemicelluloses in plant secondary cell walls. *Curr. Opin. Biotechnol.* **2019**, *56*, 97−104.

(63) Nishimura, H.; Kamiya, A.; Nagata, T.; Katahira, M.; Watanabe, T. Direct evidence for α ether linkage between lignin and carbohydrates in wood cell walls. *Sci. Rep.* **2018**, *8*, No. 6538.

(64) Balakshin, M.; Capanema, E.; Gracz, H.; Chang, H.-m.; Jameel, H. Quantification of lignin−carbohydrate linkages with high-resolution NMR spectroscopy. *Planta* **2011**, *233*, 1097−1110.

(65) Scheller, H. V.; Ulvskov, P. Hemicelluloses. *Annu. Rev. Plant Biol.* **2010**, *61*, 263−289.

(66) Chan, J. Microtubule and cellulose microfibril orientation during plant cell and organ growth. *J. Microsc.* **2012**, *247*, 23−32.

(67) Chafe, S. C.; Wardrop, A. Microfibril orientation in plant cell walls. *Planta* **1970**, *92*, 13−24.

(68) Shah, R. S.; Senanayake, M.; Zhang, H.-H.; Pu, Y.; Biswal, A. K.; Pingali, S. V.; Davison, B.; O'Neill, H. Evidence for lignin−carbohydrate complexes from studies of transgenic switchgrass and a model lignin−pectin composite. *ACS Sustainable Chem. Eng.* **2023**, *11*, 15941−15950.

(69) Wei, Y.; Hore, M. J. Characterizing polymer structure with small-angle neutron scattering: A Tutorial. *J. Appl. Phys.* **2021**, *129*, No. 171101.

(70) Petridis, L.; Schulz, R.; Smith, J. C. Simulation analysis of the temperature dependence of lignin structure and dynamics. *J. Am. Chem. Soc.* **2011**, *133*, 20277−20287.

(71) Kafle, K.; Xi, X.; Lee, C. M.; Tittmann, B. R.; Cosgrove, D. J.; Park, Y. B.; Kim, S. H. Cellulose microfibril orientation in onion (Allium cepa L.) epidermis studied by atomic force microscopy (AFM) and vibrational sum frequency generation (SFG) spectroscopy. *Cellulose* **2014**, *21*, 1075−1086.

(72) Nicolas, W. J.; Fäßler, F.; Dutka, P.; Schur, F. K. M.; Jensen, G.; Meyerowitz, E. Cryo-electron tomography of the onion cell wall shows bimodally oriented cellulose fibers and reticulated homogalacturonan networks. *Curr. Biol.* **2022**, *32*, 2375−2389.

(73) Liu, J.; Kim, J. I.; Cusumano, J. C.; Chapple, C.; Venugopalan, N.; Fischetti, R. F.; Makowski, L. The impact of alterations in lignin deposition on cellulose organization of the plant cell wall. *Biotechnol. Biofuels* **2016**, *9*, No. 126.

(74) Weng, Y.; Nagle, B.; Mueller, K.; Catchmark, J. The formation of Gluconacetobacter xylinum cellulose under the influence of the dye brilliant yellow. *Cellulose* **2019**, *26*, 9373−9386.

(75) Kai, A. The structure of the nascent fibril produced by acetobacter xylinum: The X-ray diffraction diagram of cellulose produced in the presence of a fluorescent brightener. *Makromol. Chem. Rapid Commun.* **1984**, *5*, 307−310.

(76) Atalla, R. H.; Vanderhart, D. L. Native cellulose: a composite of two distinct crystalline forms. *Science* **1984**, *223*, 283−285.

(77) Wada, M.; Okano, T.; Sugiyama, J. Allomorphs of native crystalline cellulose I evaluated by two equatorial d-spacings. *J. Wood Sci.* **2001**, *47*, 124−128.